Carbon nanotube cantilevers for next-generation sensors

Edward H. Feng* and Reese E. Jones
Sandia National Laboratories, Livermore, California 94551-0969, USA
(Received 23 November 2010; published 5 May 2011)

Researchers continue to make smaller force sensors and mechanical resonators in an effort to enhance force sensitivity and achieve higher resonant frequencies. We explore the single wall carbon nanotube cantilever as the ultimate limit of this trend. Using molecular dynamics simulations to calculate the thermal vibrational spectrum of tip displacements, we find that the quality factor of the cantilever is independent of its length. This leads to the surprising result that the intrinsic signal-to-noise ratio for a carbon nanotube cantilever improves with increased length. We discuss qualitative reasons why this result will also hold in a real carbon nanotube device.

DOI: 10.1103/PhysRevB.83.195412 PACS number(s): 61.48.De

I. INTRODUCTION

With the development of the atomic force microscope (AFM),[1] we have looked at individual atoms via the vibrations of cantilevered structures. Even though these first structures were cut by hand and were in the millimeter range, they provided the key sensing component in the revolutionary AFM. Cantilevers and other types of beams also play a crucial role in micromechanical resonators that employ vibrations to perform tasks such as mass sensing. These devices work because an attached mass causes a frequency shift in the fundamental mode of vibration.[2,3] For both force sensors and resonators, the vibrating beams have become progressively smaller.[4–9] Smaller devices vibrate faster and hence allow for faster measurements. Here, we explore the single wall carbon nanotube (CNT) as the ultimate limit for vibrating cantilevers.

Building on earlier work,[10] we use molecular dynamics (MD) simulations to study the signal-to-noise ratio (SNR) of a CNT cantilever. This sensing device is small enough to perform these simulations with full atomic resolution. At constant temperature, we first calculate the thermal vibrational spectrum of the tip displacements with MD.[11–14] Rescaling this spectrum for many lengths leads to a single master curve which implies that the quality factor is independent of length. This leads to the surprising result that the SNR increases with increasing CNT length. These MD simulations account for the intrinsic dissipation from anharmonic phonon interactions[15–19] but ignore other factors such as a gas atmosphere, surface contaminates, and realistic clamping to a substrate. This clean separation of intrinsic noise from external factors is very difficult in experiments.[20] Moreover, we argue that these other contributions do not change the primary conclusion that the SNR increases for longer CNT cantilevers.

The rest of the paper is organized in the following manner. Section II describes the beam theory employed as a coarse grain model for the CNT vibrations and clearly defines what we mean by anharmonic phonon interactions. Moreover, this section also describes the damped harmonic oscillator used to describe the thermal vibrational spectrum. In Sec. III, we define the tip vibrational spectrum and how we calculate it with MD simulations. Section IV details our results and how the SNR ratio gets better for longer CNT devices. Finally, we discuss other sources of dissipation and their effect on experiments in Sec. V.

II. THEORY

First, we consider the application of continuum beam theory and equilibrium statistical mechanics to the thermal vibrations of beams, an idea pioneered by Treacy and co-workers.[21] While we have previously discussed this theory in detail,[10] we summarize the results here for clarity and completeness. The Timoshenko beam can accurately describe the transverse vibrations of thin beams. It generalizes the Euler-Bernoulli theory that considers only normal, bending forces along the axis of the beam by also accounting for shear forces and rotational inertia. To understand the thermal vibrations of the CNT tip, we solve the governing equations in the Timoshenko theory to derive results for the tip displacement.[10]

First, using the time-independent solution, the tip of the cantilever acts as if it experiences a harmonic potential

$$U = \tfrac{1}{2} K u^2, \tag{1}$$

in which u is the displacement of the cantilever tip from mechanical equilibrium in a transverse direction and

$$K = \frac{3EI}{L^3}\frac{1}{1+3\kappa/\epsilon^2} \tag{2}$$

is an effective spring constant. Here, L is the length of the beam, the flexural rigidity EI is the product of the Young's modulus E and the area moment of inertia I of the beam, κ is a dimensionless parameter that gives the normal stiffness relative to the shear stiffness, and $\epsilon = L/\sqrt{I/A}$ is a dimensionless aspect ratio in which A is the cross-sectional area of the CNT. In Eq. (2), the second term in the product is the Timoshenko correction to Euler-Bernoulli theory, and one recovers Euler-Bernoulli when $\epsilon \to \infty$. We use Eq. (1) as the potential energy in the Gibbs-Boltzmann distribution, which implies that the ensemble average width of tip displacements is

$$\langle u^2 \rangle = \frac{k_B T}{K}, \tag{3}$$

in which T is temperature and k_B represents Boltzmann's constant.

To explore the vibrational dynamics of a nanoscale CNT, one can perform a normal mode analysis of the Timoshenko beam equations[10,22] and show the potential energy

$$U = \frac{1}{2}\sum_n K_n u_n^2$$

is a sum over modes in which u_n is the tip displacement of the nth mode. Here, the mode-dependent spring constants are

$$K_n = mN_n\omega_n^2, \tag{4}$$

in which m is the mass of the beam, N_n is a scalar coefficient, and the frequencies

$$\omega_n = \Omega_n\sqrt{\frac{EI}{m}}\frac{1}{L^{3/2}} \tag{5}$$

are proportional to Ω_n, a solution to a characteristic equation derived from the boundary condition on the beam. While N_n is calculated numerically[10] for the Timoshenko beam theory, $N_n = 1/4$ for all n in the Euler-Bernoulli theory. The quantity $M_n \equiv mN_n$ is an effective mass for each mode of the beam. For an atomistic model of a CNT, a normal mode analysis is quite complex. Here, we use the beam theory as a coarse-grained model for the transverse vibrational modes of the beam. In our previous work,[10] we compared the ensemble average displacement of each mode

$$\langle u_n^2\rangle = \frac{k_B T}{K_n}$$

with MD simulation results. While this expression accurately described the location and total intensity of each mode, the beam theory model could not describe the shape of the resonant peaks in the spectrum.[10] In particular, the shape of the primary mode deviated significantly from the impulse predicted from the beam theory and equilibrium statistical mechanics, a theory with no friction forces. This deviation implies that the modes cannot interact through a potential proportional to the squares of the atomic displacements (or the modes u_n), since this type of linear theory also gives impulse shapes for each resonance. Hence, there must be anharmonic interactions between these transverse phonon modes in which the potential consists of higher-order terms in u_n.

Since our calculations show that 97% of the intensity resides in the primary mode, it is reasonable to model this mode as a damped harmonic oscillator with a random force that results from interactions with all higher modes,

$$M\frac{d^2x(t)}{dt^2} + M\gamma\frac{dx(t)}{dt} + K_0x(t) = F(t). \tag{6}$$

Here, M, γ, and $F(t)$ are an effective mass of the oscillator, a friction coefficient, and a random force, respectively. Often times, $M\gamma$ is called the coefficient of viscous damping.

We will use the Fourier transform of Eq. (6) to describe the shape of the primary mode in the thermal vibrational spectrum. For simplicity, we suppose that functions of time such as $x(t)$ and $R(t)$ are periodically replicated over an interval τ. For a given time interval $\Delta\tau$, the functions are sampled at uniform points in time $t_j = j\Delta\tau$ for $j = 0,1,\ldots,N_\tau - 1$ for an even integer N_τ such that $\tau = N_\tau\Delta\tau$. The Fourier coefficients for a function $z(t)$ are

$$\hat{z}_n = \frac{1}{\tau}\int_0^\tau z(t)e^{-i\omega_n t}\,dt \approx \frac{1}{N_\tau}\sum_{j=0}^{N_\tau-1} z_j e^{-i\omega_n t_j}$$

for the discrete set of frequencies $\omega_n = 2\pi n/\tau$ for integers n such that $N_\tau/2 < n \leqslant N_\tau/2$. For the damped harmonic oscillator in Eq. (6), one can take the Fourier transform and show that the spectrum $|\hat{x}_n|^2$ in the limit as $\tau\to\infty$ is proportional to the continuous response function

$$g(\omega) = \frac{\omega_0^4}{\left(\omega_0^2-\omega^2\right)^2 + \omega^2\omega_0^2Q^{-2}}, \tag{7}$$

in which $\omega_0 = \sqrt{K_0/M}$ denotes the fundamental frequency of the oscillator and $Q = \omega_0/\gamma$ is the quality factor. The constant ω_0^4 appears in the numerator so that $g(0) = 1$. It is useful to approximate[23] this function near its peak by using $\omega_0^2 - \omega^2 = (\omega_0+\omega)(\omega_0-\omega)$ and setting $\omega = \omega_0$ in Eq. (7) except for the term $\omega_0 - \omega$. This approximate response function

$$g_a(\omega) = \frac{\omega_0^2}{4\left(\omega_0-\omega\right)^2 + \omega_0^2Q^{-2}} \tag{8}$$

reaches half its peak value at $\omega = \omega_0 \pm (\Delta\omega/2)$ when the width has a value $\Delta\omega = \omega_0/Q$. This is not true for the full response function in Eq. (7). Moreover, $g_a(\omega)$ becomes a better approximation for $g(\omega)$ near ω_0 for larger Q. Hence, the often cited definition $Q = \omega_0/\Delta\omega$ only applies to the full response function in Eq. (7) when Q is large.

In the Fourier domain, the fluctuation-dissipation theorem gives the ensemble average properties of the force

$$\langle|\hat{F}_n|^2\rangle = \frac{M\gamma k_B T B}{\pi},$$

in which $B = 2\pi/\tau$ is sometimes called the bandwidth.[2,24] This implies the ensemble average spectrum is

$$\langle|\hat{x}_n|^2\rangle = \frac{2k_BTB}{K_0^2}\frac{M\gamma}{2\pi}g(\omega_n).$$

The coefficient of viscous damping $M\gamma$ is not directly measurable in an experiment. However, using $M = K_0/\omega_0^2$ and $\gamma = \omega_0/Q$, one can write the coefficient of viscous dissipation

$$\mathcal{R} \equiv \frac{M\gamma}{2\pi} = \frac{K_0}{2\pi\omega_0 Q} \tag{9}$$

in terms of the experimentally measurable quantities K_0, ω_0, and Q.[24] We show that $\mathcal{R}$ can be measured in our MD simulations in the same manner as Viani *et al.*[24] did for their experiments.

The frequency-dependent SNR is the ratio of the tip displacement and the error induced by thermal and detector noise

$$\mathrm{SNR} = \frac{\frac{F(\omega)}{K_0}g(\omega)}{\sqrt{\frac{4k_BT\mathcal{R}B}{K_0^2}g^2(\omega) + (\text{detector noise})^2}}. \tag{10}$$

Here, an extra factor of 2 arises in the thermal noise due to the equal contribution from positive and negative frequencies to

the spectrum. For an ideal sensor with no detector noise, the SNR scales as

$$\mathrm{SNR} \sim (k_B T \mathcal{R})^{-1/2}.$$

For certain measurements taken at a fixed temperature, the only way to enhance the SNR is to decrease the coefficient of viscous damping $\mathcal{R}$.

III. COMPUTATIONAL METHODS

To understand the SNR of a CNT device, we define the thermal vibrational spectrum. If $u(t_j)$ is the displacement from mechanical equilibrium of the tip of a CNT cantilever in one of two transverse dimensions, then the thermal vibrational spectrum is

$$h(\omega_k) = \langle |\hat{u}(\omega_k)|^2 \rangle_{NVT},$$

in which the angular brackets denote an average over the canonical ensemble at constant number of particles N, volume V, and temperature T. To evaluate this statistical mechanical average, we first sample the canonical ensemble with MD and the Andersen thermostat[25] to obtain a set of states from the canonical ensemble. Then, these states provide initial conditions for the calculation of trajectories at constant energy with no thermostat. This method for probing the dynamics of a system at constant temperature is standard in the study of liquids.[26]

In this work, we study (10,10) CNTs of length $L = 10$, 20, 50, and 100 nm at temperature $T = 300$ K. The carbon atoms interact through a multibody Tersoff potential.[27,28] We make the CNT a cantilever by fixing the positions of carbon atoms at one end of the tube. This zero-temperature substrate represents ideal clamping because the CNT does not exchange energy with the substrate atoms. Moreover, our simulations do not contain free gas molecules or attached contaminants on the surface of the defect-free tube. Additional details about the construction of a CNT cantilever and the sampling methods can be found in a previous work.[10] For all tube lengths, we obtain 30 samples from the canonical ensemble, run trajectories of 10 ns and use $\Delta\tau = 10$ fs to calculate the thermal vibrational spectrum.

IV. RESULTS

First, we check the equilibrium properties of the CNT as a function of length. In Fig. 1, we show the equilibrium squared tip displacement $\langle u^2 \rangle \equiv \langle u^2(t_j = 0) \rangle$ for MD and beam theory as a function of length L at $T = 300$ K. In showing the predictions of Timoshenko and Euler-Bernoulli theory, we approximate the CNT as an infinitely thin shell which implies $\epsilon = \sqrt{2}L/R$ with radius $R = 0.7$ nm. Moreover, we use the estimate $EI = 4.0806 \times 10^{-25}$ N m^2 obtained by analyzing $\langle u^2 \rangle$ as a function of temperature T in previous work.[10] These quantities are substituted into the expression for $\langle u^2 \rangle$ in Eq. (3), which requires the spring constant in Eq. (2). Both the Timoshenko and Euler-Bernoulli predictions agree well with the equilibrium MD simulations at various lengths in Fig. 1. The two beam theories differ only slightly for small L, high aspect-ratio tubes since the inclusion of shear stress and rotational inertia in the Timoshenko theory has the greatest

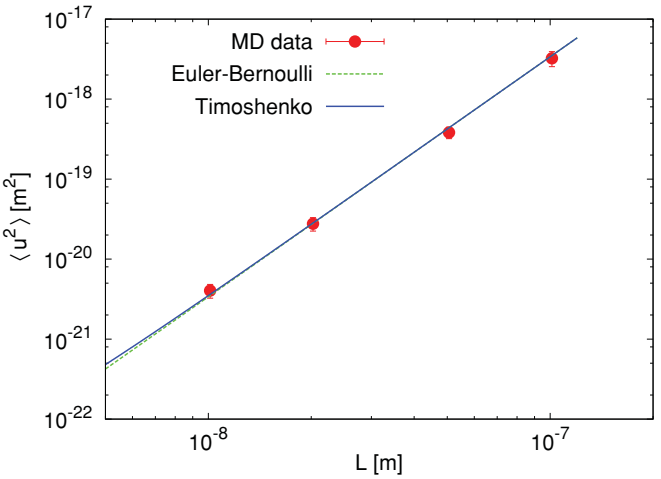

FIG. 1. (Color online) The equilibrium squared tip displacement $\langle u^2 \rangle$ as a function of length L at a temperature $T = 300$ K. Equations (3) and (2) provide theoretical results for the Timoshenko and Euler-Bernoulli ($\epsilon \to \infty$) beam theories.

effect for low aspect-ratio beams. Figure 1 not only supports our use of continuum beam theory to describe a CNT, but also suggests that the flexural rigidity is independent of tube length in our simulations using the Tersoff potential.

After examining the equilibrium properties of the CNT, we now consider the thermal vibrational spectrum. Figure 2

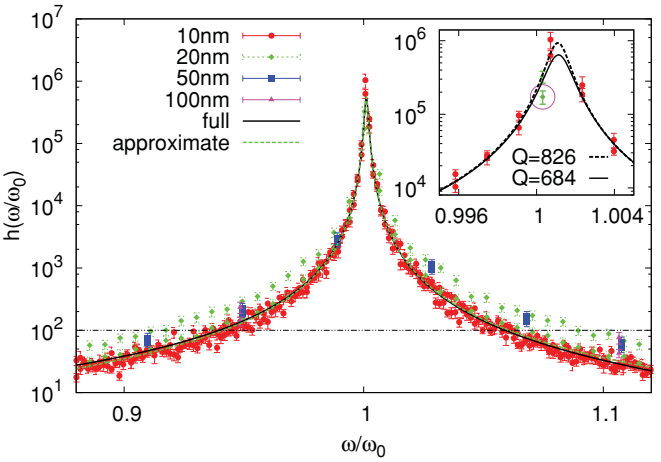

FIG. 2. (Color online) The amplitude of the vibrational spectrum as a function of frequency for four different CNT lengths. The discrete data points included both transverse dimensions which can display small differences due to thermal fluctuations. For each spectrum, we rescale the amplitude by the zero frequency amplitude and frequency by the Timoshenko result for fundamental frequency given in Eq. (5). We fit the response function for a damped harmonic oscillator to the data for points above the horizontal dashed-dotted line and obtain a quality factor $Q = 684$. The inset illustrates the sensitivity of the fit to data near the peak. By removing one of the $L = 20$ nm data (circled), the fit reaches the maximum of the $L = 10$ nm data and the estimated Q increases to 826.

shows that the spectrum $h_L(\omega_k)$ for various lengths L can be expressed as

$$h_L(\omega_k) = h_L(0)\,\bar{h}\left(\frac{\omega_k}{\omega_0(L)}\right)$$

in terms of a scaling function $\bar{h}[\omega_k/\omega_0(L)]$. We show this by rescaling the amplitude of $h_L(\omega_k)$ by its zero frequency value and ω_k by the fundamental frequency from Timoshenko beam theory ω_0 in Eq. (5). For frequencies near the fundamental mode, the thermal vibrational spectrum from four different lengths spanning an order of magnitude collapse onto $\bar{h}[\omega_k/\omega_0(L)]$. The collapse of the data is particularly remarkable for values larger than 1000.

To understand this scaling function, we consider the response function of a damped harmonic oscillator in Eq. (7) and fit

$$G(\omega : A,\omega_0,Q) = Ag(\omega : \omega_0,Q)$$

for parameters A, ω_0, and Q to data near the peak $\bar{h}(\omega_k/\omega_0) > 100$. The fit is relatively insensitive to this lower bound. In Fig. 2, we show the agreement of both the full and approximate response functions, Eqs. (7) and (8), respectively, using the fitted value $Q = 684 \pm 103$ with the data, which validates the use of only points near the peak. This value for Q is consistent with previous MD simulations[12] at $T = 300$. Moreover, $Q = 684$ is in the high end of the range of experimental measurements,[5,29,30] an expected result since our simulations do not consider sources of dissipation that could potentially lower Q. The fit is most sensitive to data near the peak. Unfortunately, this data is difficult to obtain because the difference between adjacent frequencies scales inversely with trajectory length. To illustrate this sensitivity, we removed one data point (circled in the inset of Fig. 2) from the fitted data and the estimated quality factor changes to $Q = 826 \pm 128$ without significantly changing the other fitted parameters. Moreover, there are uncertainties in ω since calculating the frequencies requires the flexural rigidity EI estimated from equilibrium simulations. The 2% errors in frequencies could cause relative misalignment of the data sets for the various lengths. Lastly, the fitted value $\omega_0 = 1.001 \pm 0.006$ is very close to the value $\omega_0 = 1$ one would expect if the Timoshenko beam theory accurately describes the fundamental frequency of the CNT.

The collapse of the thermal vibrational spectrum for many CNT lengths in Fig. 2 implies a scaling of quality factor with length

$$Q \sim L^{-\alpha}.$$

If we rescale the frequency of the response function in Eq. (7) by ω_0 with $\bar{\omega} = \omega/\omega_0$, then the function

$$g(\bar{\omega}) = \frac{1}{(1-\bar{\omega}^2) + \bar{\omega}^2 Q^{-2}}$$

can only describe the collapse of the vibrational spectrum if Q is independent of length, or $\alpha \approx 0$.

With this new result for the quality factor, we now analyze the SNR in Eq. (10) for a CNT sensor. For an ideal sensor with no detector noise, SNR $\sim (k_B T\mathcal{R})^{-1/2}$ so higher fidelity measurements can result from lower temperatures T or a lower

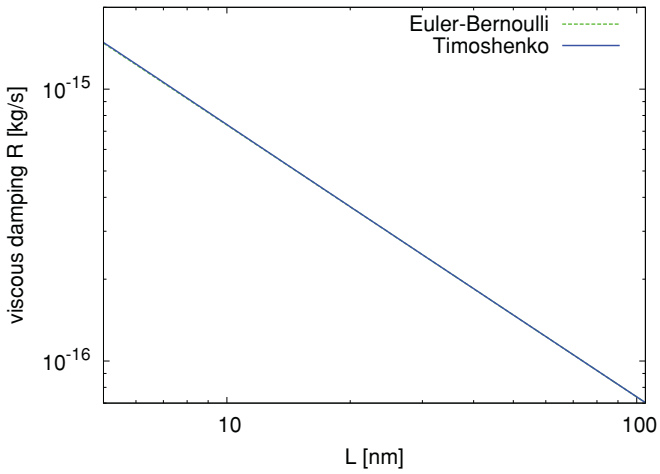

FIG. 3. (Color online) The coefficient of viscous damping $\mathcal{R}$ as a function of length L for a CNT based on beam theory and the quality factor obtained in MD simulations. The SNR for an ideal CNT sensor scales with $\mathcal{R}^{-1/2}$. The Timoshenko and Euler-Bernoulli theory are almost identical for all length displayed and both give $\mathcal{R} \sim L^{-1}$.

coefficient of damping. Since it is not possible to measure the coefficient of viscous damping directly in MD simulations, the expression $\mathcal{R} = K_0/(2\pi\omega_0 Q)$ allows us to estimate this quantity through K_0, ω_0, and Q. The fundamental frequency ω_0 is given in Eq. (5) and requires an estimate of the flexural rigidity EI obtained from previous work.[10] Moreover, K_0 in Eq. (4) needs a numerical calculation to determine the scalar N_0 as a function of length. Lastly, we use $Q = 684$ independent of length. Figure 3 shows how $\mathcal{R}$ decreases with increasing length for both Timoshenko and Euler-Bernoulli beam theory. Even for small L, the Timoshenko result is almost identical to the Euler-Bernoulli theory since both K_0 and ω_0 decrease with the added effects of rotational inertia and shear stress in the Timoshenko theory.

To understand how the coefficient of viscous damping and SNR scale with length, we require a few results from beam theory. Equations (4) and (5) imply that $K_0 \sim L^{-3}$ and $\omega_0 \sim L^{-2}$, so the coefficient of viscous damping scales with length as $\mathcal{R} \sim (K_0/\omega_0) \sim L^{-1}$. This is contrary to experiments on silicon-based AFM cantilevers,[24] a discrepancy we discuss in the next section. Here, SNR $\sim \mathcal{R}^{-1/2} \sim L^{1/2}$ implies the SNR increases with increasing length for an ideal CNT sensor. Lastly, we emphasize the term "coefficient of viscous damping" in this context arises from the intrinsic anharmonic phonon interactions discussed in Sec. II for the CNT, not from interactions with an external viscous medium such as a gas or liquid.

V. DISCUSSION

As we discussed in the theory section, the MD results for a CNT cantilever capture the effect of anharmonic phonon interactions on the fluctuations and dissipation of the fundamental mode. However, these simulations do not account for other sources of dissipation in real systems.[19,20,30,31]

The first important source arises from gas friction. In our simulations, there are no gas molecules that collide with the beam and reduce Q through the momentum transfer between

CNT and gas molecules. Previous theoretical work[2] gives this dissipation

$$Q_{\rm gas}^{-1} = \frac{pA_{\rm surf}}{M\omega_0 v}$$

in terms of an effective mass for the beam M, the frequency of the resonator which we take to be the fundamental ω_0, the thermal velocity of the gas v, the ambient pressure p, and the surface area of the resonator $A_{\rm surf}$. This expression comes from the kinetic theory result that the drag force on body moving through a dilute gas is $(pA_{\rm surf}/v)V$, in which V is the velocity of the body. The effective mass is determined by beam theory so that $\omega_0 = \sqrt{K_0/M}$. As mentioned earlier, the Euler-Bernoulli theory gives $M = m/4$ in which m is the mass of the CNT cantilever, whereas the effective mass in the Timoshenko theory is mN_0 in which the numerical factor N_0 in Eq. (4) depends on the aspect ratio of the beam.[10]

In our CNT simulations, the cross-sectional area remains the same while the length of the beam changes. This implies

$$Q_{\rm gas}^{-1} \sim L^2 \tag{11}$$

so the dissipation increases for longer CNTs. Physically, the longer tubes provides more surface area for collisions with gas molecules. Substituting this result into Eq. (9) gives $\mathcal{R} \sim L$ for the coefficient of viscous dissipation. This implies that SNR $\sim L^{-1/2}$ would decrease with increasing length. However, we now consider the magnitude of this effect by comparing $Q_{\rm gas}^{-1}$ for a 100-nm CNT with a microscale silicon cantilever of length 10 μm, a size on the small end of devices studied by Hansma and co-workers.[24,32] Assuming the MD and experimental silicon cantilevers have approximately the same aspect ratio, the microscale cantilever is bigger than the CNT in all three dimensions by a factor $\ell = 100$. Note that the analysis that led to Eq. (11) assumes only one-dimensional changes. This implies

$$\frac{Q_{\rm gas,CNT}^{-1}}{Q_{\rm gas,Si}^{-1}} \sim \ell^{-1},$$

so the dissipation decreases by two orders of magnitude for the CNT cantilever. From previous experiments on silicon cantilevers in air, Walters *et al.*[32] obtain $Q_{\rm Si} \approx 130$. Let us assume that the dissipation in the silicon cantilevers is dominated by gas friction $Q_{\rm gas,Si} \approx Q_{\rm Si}$. If different sources of damping act independently, the total dissipation is $Q^{-1} = Q_{\rm beam}^{-1} + Q_{\rm gas}^{-1}$. For the CNT, this changes Q from 684 to 649 so the gas friction does not change the order of magnitude of the quality factor. This gas friction can be made much smaller by reducing the air pressure in the system.

A second commonly cited source of dissipation in vibrating beams is surface contamination from absorbed gas molecules, structural defects in the crystal structure of the tube, or broken carbon-carbon bonds.[8,19,30] To estimate its magnitude, recall that the quality factor Q is the ratio of the elastic energy initially stored in the resonator to the energy dissipated per cycle. Since the initial energy is proportional to volume while the energy dissipated due to surface contaminants must scale as surface area,

$$Q_{\rm surface}^{-1} \sim L^{-1}.$$

This simple scaling argument has been proposed to explain the linear scaling of Q with linear dimension over many orders of magnitude.[30] Absorption of gas molecules will be minimal in low-pressure operating environments. Moreover, advances in synthetic methods for making single wall CNTs will reduce defects, broken bonds, and external surface contamination due to the fabrication environment. While surface contaminants might reduce the overall quality factor, the scaling $Q \sim L$ implies that $\mathcal{R} \sim L^{-2}$ instead of $\mathcal{R} \sim L^{-1}$. This implies SNR $\sim L$ instead of SNR $\sim L^{1/2}$ for the SNR, so longer CNTs still make better sensors in this case.

A third source of dissipation in cantilevered beams arises from clamping to the substrate. Photiadis and Judge developed an elegant theory for clamping loss in rectangular cantilevers using Euler-Bernoulli theory.[33,34] It is straightforward to generalize their scaling result to a beam of arbitrary cross section

$$Q_{\rm clamp}^{-1} = c\frac{L^5}{I\sqrt{I/A}}. \tag{12}$$

Here, I and A are the area moment of inertia and cross-sectional area, respectively, while c is a numerical coefficient. For a cylindrical beam of radius R, this clamping loss scales $Q^{-1} \sim (L/R)^5$. The smaller fraction of surface area consumed by clamping for large aspect-ratio beams results in smaller dissipation. The coefficient c in Eq. (12) is order unity for a rectangular beam.[33] If this factor is the same order for a cylindrical structure, the clamping dissipation is negligible for CNTs. For a hollow cylinder, the dissipation is even smaller than for a solid cylinder since $I/A \sim R^2$ for both structures, but the area moment of inertia is much smaller for a hollow structure.

We now compare our MD results on dissipation and Q with the experiments of Hansma and co-workers.[24,32] They looked at the thermal vibrations in air of a set of silicon nitride cantilevers with the same rectangular cross sections and lengths ranging from 15 to 55 μm. From Fig. 3(c) of their results,[32] we estimate a dissipation $Q^{-1} \sim L^{\alpha}$ with $\alpha \approx 1.46$. We believe this scaling results from a combination of gas friction and surface effects. With a reduced pressure atmosphere and defect-free synthetic procedures, these two factors might not affect a CNT cantilever.

In addition, the work of Jensen, Zettl and co-workers[29] on doubly clamped CNTs demonstrates that quality factors of $Q \approx 1000$ are achievable in real devices. Although Fig. 3 in that reference shows a correlation of Q with length, there are numerous instances over the CNT lengths studied of devices with $Q \approx 1000$. This is despite potentially underestimating the quality factors by up to 10% and having approximately twice the dissipation due to clamping loss of a cantilever. (Although not explicitly stated, it is assumed that the measurements were taken in vacuum and thus also missing the effects of gas friction.)

VI. CONCLUSION

To understand the signal-to-noise ratio of a carbon nanotube sensor, we studied the thermal vibrational spectrum of tip displacements with molecular dynamics. Our results showed that the intrinsic quality factor $Q \approx 700$ was length independent.

This also led to the surprising conclusion that the signal-to-noise ratio of an ideal CNT sensor SNR $\sim L^{1/2}$ increased with increasing length. Using displacement detection techniques with low detector noise and high accuracy, such as those stemming from the field emission properties of a CNT,[3] experiments could directly measure the thermal vibrational spectrum and potentially confirm that $Q \approx 700$ independent of length. Moreover, high-quality synthetic methods and a low pressure environment would minimize the dissipative effects from surface defects and gas friction, allowing one to measure the intrinsic dissipation from anharmonic interaction between vibrational modes.

ACKNOWLEDGMENTS

We would like to acknowledge the support of the Laboratory Directed Research and Development program at Sandia National Laboratories. Sandia is a multiprogram laboratory operated by Sandia Corporation, a Lockheed Martin Company, for the United States Department of Energy under Contract No. DE-ACO4-94AL85000.

*ehfeng@sandia.gov

[1] G. Binnig, C. F. Quate, and C. Gerber, Phys. Rev. Lett. **56**, 930 (1986).
[2] K. L. Ekinci, Y. T. Yang, and M. L. Roukes, J. Appl. Phys. **95**, 2682 (2004).
[3] K. Jensen, K. Kim, and A. Zettl, Nat. Nanotechnol. **3**, 533 (2008).
[4] A. N. Cleland and M. L. Roukes, Appl. Phys. Lett. **69**, 2653 (1996).
[5] P. Poncharal, Z. L. Wang, D. Ugarte, and W. A. D. Heer, Science **283**, 1513 (1999).
[6] A. N. Cleland and M. L. Roukes, Sens. Actuators, A **72**, 256 (1999).
[7] V. Sazonova, Y. Yaish, H. Ustunel, D. Roundy, T. A. Arias, and P. L. McEuen, Nature (London) **431**, 284 (2004).
[8] H. B. Peng, C. W. Chang, S. Aloni, T. D. Yuzvinsky, and A. Zettl, Phys. Rev. Lett. **97**, 087203 (2006).
[9] X. L. Feng, R. He, P. Yang, and M. L. Roukes, Nano Lett. **7**, 1953 (2007).
[10] E. H. Feng and R. E. Jones, Phys. Rev. B **81**, 125436 (2010).
[11] B. I. Yakobson, C. J. Brabec, and J. Bernholc, Phys. Rev. Lett. **76**, 2511 (1996).
[12] H. Jiang, M. F. Yu, B. Liu, and Y. Huang, Phys. Rev. Lett. **93**, 185501 (2004).
[13] L. Wang and H. Hu, Phys. Rev. B **71**, 195412 (2005).
[14] J.-Y. Hsieh, J.-M. Lu, M.-Y. Huang, and C.-C. Hwang, Nanotechnology **17**, 3920 (2006).
[15] A. A. Maradudin and A. E. Fein, Phys. Rev. **128**, 2589 (1962).
[16] A. A. Maradudin, A. E. Fein, and G. H. Vineyard, Phys. Status Solidi **2**, 1479 (1962).
[17] H. Michel and M. Wagner, Phys. Status Solidi B **85**, 195 (1978).
[18] R. Lifshitz and M. L. Roukes, Phys. Rev. B **61**, 5600 (2000).
[19] A. N. Cleland and M. L. Roukes, J. Appl. Phys. **92**, 2758 (2002).
[20] P. Mohanty, D. A. Harrington, K. L. Ekinci, Y. T. Yang, M. J. Murphy, and M. L. Roukes, Phys. Rev. B **66**, 085416 (2002).
[21] M. M. J. Treacy, T. W. Ebbesen, and J. M. Gibson, Nature (London) **381**, 678 (1996).
[22] T. Huang, J. Appl. Mech. **28**, 579 (1961).
[23] R. P. Feynman, *The Feynman Lectures on Physics: Volume 1* (Addison-Wesley, Boston, 1963), Chaps. 21–23.
[24] M. B. Viani, T. E. Schaffer, A. Chand, M. Rief, H. E. Gaub, and P. K. Hansma, J. Appl. Phys. **86**, 2258 (1999).
[25] H. C. Andersen, J. Chem. Phys. **72**, 2384 (1980).
[26] M. P. Allen and D. J. Tildesley, *Computer Simulation of Liquids* (Clarendon, New York, 1989).
[27] J. Tersoff, Phys. Rev. B **37**, 6991 (1988).
[28] J. Tersoff, Phys. Rev. Lett. **61**, 2879 (1988).
[29] K. Jensen, Ç. Girit, W. Mickelson, and A. Zettl, Phys. Rev. Lett. **96**, 215503 (2006).
[30] K. Jensen, H. Peng, and A. Zettl, *2006 International Conference on Nanoscience and Nanotechnology* (IEEE, Piscataway, NJ, 2006).
[31] K. L. Ekinci and M. L. Roukes, Rev. Sci. Instrum. **76**, 061101 (2005).
[32] D. A. Walters, J. P. Cleveland, N. H. Thomson, P. K. Hansma, M. A. Wendman, G. Gurley, and V. Elings, Rev. Sci. Instrum. **67**, 3583 (1996).
[33] D. M. Photiadis and J. A. Judge, Appl. Phys. Lett. **85**, 482 (2004).
[34] J. A. Judge, D. M. Photiadis, J. F. Vignola, B. H. Houston, and J. Jarzynski, J. Appl. Phys. **101**, 013521 (2007).